



Experimental validation of numerical simulation on deformation behaviour induced by wire arc additive manufacturing with feedstock SS316L on substrate S235

Siti Nursyahirah Ahmad¹ · Yupiter HP Manurung¹ · Mohd Shahrizan Adenan¹ · Farazila Yusof² · Muhd Faiz Mat¹ · Keval P Prajadhiana¹ · Zaidi Minggu¹ · Martin Leitner³ · Salina Saidin⁴

Received: 25 June 2021 / Accepted: 2 November 2021 / Published online: 2 December 2021
© The Author(s), under exclusive licence to Springer-Verlag London Ltd., part of Springer Nature 2021

Abstract

This fundamental research aims to analyse the effect of heat transfer coefficients, plasticity model of evolved material properties and simplified meshing strategy on substrate deformation induced by wire arc additive manufacturing (WAAM) process with dissimilar materials based on experiment and numerical simulation. Throughout the experiment, stainless steel wire SS316L was used as feedstock to build a five-layer and three-string component on an 8-mm-thick low carbon steel S235 as substrate plate by means of a robotic GMAW system with pure argon as shielding gas and diagonal clamping. In order to define heat transfer coefficients by adjusting simulation to experimental results, the transient thermal distribution was to be measured at specific points located in the component layer using Type K thermocouple inserted during the process and on the substrate implanted beforehand. For modelling and simulation, a non-linear thermo-mechanical method was applied in which the component was modelled using rectangular element shape with optimized hexagonal mesh size obtained through sensitivity analysis in accordance to actual specimen geometry and clamping condition. Non-linear isotropic hardening rule with von Mises yield criterion and temperature-dependent material properties was implemented into the simulation which were generated by means of advanced material modelling software based on elemental composition of evolved component characterized using SEM/EDX. For numerical and experimental validation purpose, substrate deformation was measured using coordinate measurement machine before and after the process. It can be concluded that the result of the computed substrate deformation showed an acceptable agreement compared to experiment within the range of error between 0.5 and 27.5% at each specific measurement points and 10.1% as average single error. This basic investigation can be enhanced in the case where cost-effective WAAM application with dissimilar materials towards single-piece substrate component is concerned.

Keywords Distortion · Numerical computation · WAAM · SS316L

1 Introduction

Additive manufacturing (AM) has become an important manufacturing process in recent years especially for custom-made workpieces [1–3]. Various studies have predicted that metallic AM (MAM) will play a profound role in the manufacturing industry of the future [4–6]. There are various advantages compared to conventional processes; for instance, AM can replace conventional manufacturing processes such as machining that often requires a large amount of material usage and cannot meet the continuous demands for low cost and sustainability in a modern industry. MAM, which consists of a substrate, feedstock, motion system and heat source, is regarded as an excellent choice for producing parts or components made

✉ Yupiter HP Manurung
yupiter.manurung@uitm.edu.my

¹ Smart Manufacturing Research Institute (SMRI) and School of Mechanical Engineering, Universiti Teknologi MARA (UiTM), Shah Alam, Malaysia

² Centre of Advanced Manufacturing & Material Processing (AMMP Centre), University of Malaya, Kuala Lumpur, Malaysia

³ Institute of Structural Durability and Railway Technology, Graz University of Technology, Graz, Austria

⁴ NDT Lab and Metrology Lab, Nusantara Technologies Sdn. Bhd, Shah Alam, Malaysia

of high-end materials such as titanium or aluminium alloys because of the high ratio of buy-to-fly.

Basically, powder-feed, powder-bed and wire-feed systems are the three different classification of MAM processes [7–9]. Due to high deposition rate, wire-feed system using wire arc additive manufacturing (WAAM) is considered as one of auspicious breakthrough which allows effective manufacturing operation on large-scale component with medium complexity and low-volume metal workpiece [10–13]. Principally, WAAM comprises a combination of heating source from electric arc with a feeding system of metallic wire which enables the component production layer-by-layer through building strategy by means of welding technology such as gas metal arc welding (GMAW). In many research outcomes, metal component produced by WAAM can reach the tensile strength of casting or forging part [14–16].

Unfortunately, when compared to additive technologies with powder-bed or beam melting, WAAM produces a poor surface finish and dimensional accuracy. Hence, it is critical to pay attention to how each process parameter interacts with material properties in order to produce a high-quality product. Numerical computation can be used to make an estimate that takes thermal-mechanical parameters and diverse boundary conditions into account [17, 18]. Basically, numerical simulation of WAAM carries out similar approaches applied in the multi-layered welding simulation due to phenomenon of heat transfer from the arc to the molten pool of workpiece by heat source. Therefore, the heat propagation in GMAW-based MAM is highly non-linear in nature because of the existence of multiple fusions, solidification and transformation of phases [19, 20].

By adapting similar concept of multi-passes of arc welding process, WAAM allows high deposition rate for flexible and rapid creations of complex metal components. Unfortunately, welding distortion tends to emerge from this flexibility in many cases due to thermal gradients that are massive within the workpiece during process. The welding process causes deformation or changes in shape in the entire structure, including the substrate, which is due to local expansion and contraction throughout the heating and cooling cycle of the process. Welding distortion is a problem in the manufacturing process that can have a big impact on assembly accuracy, appearance and component strength.

The residual stress and distortion can be predicted via numerical computation, allowing mitigating strategies to be developed. An initial estimation for various temperature-dependent effects should be made with consideration of thermal-mechanical boundary conditions [21, 22]. Based on the previous experimental work, deformation analysis on WAAM process using thermo-mechanical numerical calculation was performed, and the results compared to experiments stated that the simulation using simplified bead modelling exhibited good consistency with error percentage of 17.3% and the computational time was greatly reduced [23].

A numerical model for semi-finished WAAM products using commercial FEM software analysed the effect of wire

feeding speed and temperature distribution on the result outcomes. The conclusion can be drawn that the orientation position of bead deposition had a considerable impact on distribution of transient temperature and component geometry [24]. Other analysis of WAAM deformation of a substrate made of aluminium was carried out and compared by using FEM with a moving heat source resulting in a relative error of approximately 20% [25]. Filippo et al. reported that the higher inaccuracy of WAAM simulation with percentage errors of 26% was due to the inconsideration of the actual material data from literature and experimental work [26]. However, deformation induced by WAAM models using actual material modelling were seldom simulated and presented in past literature works.

Electromagnetism, heat and mass transmission, metallurgy and mechanics are among the physical phenomena involved in the WAAM process. Heat transfer, including conduction and convection, and mechanical responses are all taken into account in this study. Because the holding duration over a specific high temperature is relatively short, creep behaviour is expected to have a limited impact on residual stress and deformation. Because stainless steel SS316L has a stable austenitic structure in the temperature range of 20 to 1450 °C, strain increment caused by transformation of phase is ignored [27]. In this thermo-mechanical analysis of WAAM process, the temperature-dependent mechanical properties such as Young's modulus, Poisson's ratio, yield strength and thermal expansion coefficient are employed. To calculate the stress, the thermal elastic-plastic material model based on von Mises yield criterion and linear isotropic strain hardening rule are implemented.

Based on the reviewed literatures, it can be revealed that not many researchers investigated WAAM process which emphasizes on dissimilar materials such as SS316L and S235 as component and substrate, adjustment of heat transfer coefficients based on thermal distribution in and outside weld pool, implementation of plasticity model of evolved component material property and simplified meshing elements with sensitivity analysis. Due to these facts, this research was carried out to investigate a thick-walled WAAM structure with five layers and three strings by using numerical computation validated by a series of experiments. The main objectives are to observe the influence of the actual material data used in the experiment and other process parameters on the deformation behaviour of WAAM model with dissimilar material. The research started with the numerical computation using evolved material model property of SS316L measured after experiment using automated welding system. Further, heat transfer coefficient was adjusted and calibrated by comparing the curve in cooling phase of the experimental and simulation result. For this purpose, the temperature distributions were measured on substrate and inside the weldment right after the weld pool was formed. Next, to achieve optimized mesh numbers and accuracy, mesh sensitivity analysis of WAAM model based on maximum temperature

was conducted. As points of conclusion and further recommendation, results between experiment and FEM simulation on substrate deformations will be validated, analysed and discussed.

2 Experimental set-up and procedures

The set-up and procedure for this study obtained by WAAM process consist of characterization of material stainless steel SS316L using SEM-EDX analysis and distortion measurement using coordinate measurement machine (CMM). A series of comprehensive WAAM experiments were built with optimum welding parameters, and workpieces were manufactured by depositing successive layer-by-layer of material on a low carbon steel substrate S235. The used filler material with 1.2 mm diameter is a standard filler for structural steel welding, the designation of which is austenitic stainless steel ER316LSi in accordance with AWS standard.

The test samples were manufactured additively by superimposing five layers with three strings in which a 120 s pause was set between each layer deposition to allow the material to be partially cooled. In the execution of the workpieces, an arc length of 3 mm between the wire tip and work surface was set. The ABB IRB 2400/16 is the assigned robotic welding machine applied for the entire experimental process and the KEMMPI Pro Evolution ProMIG 540MXE as the power source as shown in Fig. 1.

The process parameters were executed based on previously successful research work performed by setting GMAW parameters such as arc current (A), voltage (V), travel speed (v) and wire feed rate (wfr) as tabulated in Table 1.

Figure 2 illustrates Type-K thermocouple at the determined positions in the feedstock and on the substrate. For the calibration of the simulated WAAM models, real measured temperature history was recorded by using data logger ALMEMO 2890-9d. Immediately after the welding arc, the thermocouple TC2 was

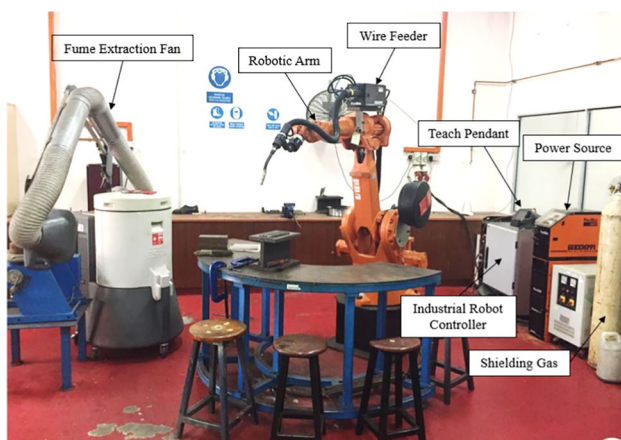


Fig. 1 ABB IRB 2400/16 robotic welding machine and KEMMPI ProMIG 540MXE

inserted gradually into the weld pool. The gradual insertion of thermocouple was aimed to maintain the solid wire tip for measuring the temperature within the component. The recording cycle of the thermocouples began after the solidification of the filler material. This enabled the transient temperature field to be analysed for designated layers and positions in the WAAM components during welding, cooling and reheating by the following layers. The recorded temperature cycles were adjusted in the FEM model to define major heat transfer coefficients.

As verification technique for distortion measurement, CMM as depicted in Fig. 3 was used to determine the pre-condition substrate displacement prior to the experimental work and post-condition deformation after the accomplishment of WAAM procedure.

The chemical composition of evolved WAAM components with wire feedstock of Oerlikon Inertfil 316LSi was analysed using SEM/EDX Hi-Tech Instrument SU3500 to develop temperature-dependent material properties. Figure 4 demonstrates the specimen sample and SEM/EDX analysis results. Table 2 summarizes the results of chemical composition of evolved component material which lays within the acceptable range of the SS316L filler material's applicable standard. Material modelling of actual component material was developed using advanced material tool JMATPRO based on results of elemental compositions.

3 Non-linear thermo-mechanical simulation for WAAM process

The general-purposed FEM programme MSC Marc/Mentat was applied to execute the coupled thermo-mechanical numerical simulation in order to conduct the thermal calibration and forecast the substrate distortion of the WAAM structure. The procedure and simulation set-up require geometrical, material and heat source model as well as thermal calibration.

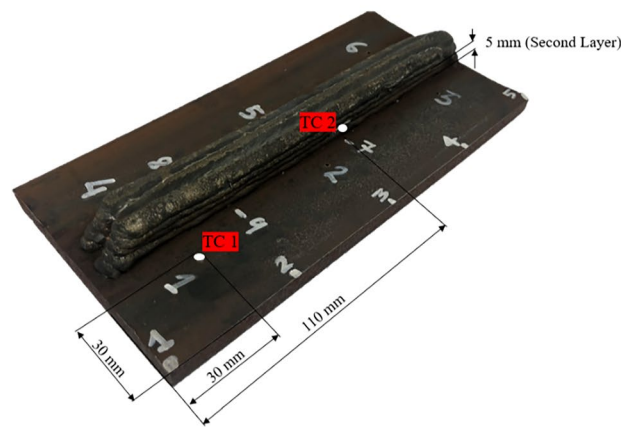
3.1 Model for geometry and material

Figure 5 shows a 3D-solid FE model of a thick-walled WAAM component made up of three sets of geometries: a table, a base plate and multi-layers WAAM beads. The

Table 1 Experimental parameters for thick-walled WAAM

WAAM process parameters	Value
Current (I)	172 A
Voltage (V)	19.8 V
Travel speed (v)	5 mm/s
Wire feed rate (wfr)	6.4 m/min
Shielding gas flow rate	15 l/min
Shielding gas composition	100% argon

Fig. 2 Schematic representation of the thermo-coupled position in component and on substrate



base plate model has a dimension of 200 mm in length, 97.5 mm in width and 8 mm in height. The model of multi-pass deposited wall was designed with a rectangular-shaped weld bead of 190 mm in length with three strings and five layers.

Bead model of WAAM geometry is critical for accurate reconstruction of the actual structure and good numerical calculation convergence. The strategy of modelling made use of a simple rectangular shape, which can reduce pre-processing effort and CPU time. To model the filler material, the element birth approach or activation element was used, in which all elements of the weld bead were deactivated at the start of the analysis and then activated progressively as the heat source moved [29–32].

Two clamps on the top substrate and table in a cross-diagonal configuration were acted as mechanical boundary conditions. The holding force of the structural clamp was set to 100 N. The clamping force on the base plate is seen in negative y-directions in Fig. 6. Equilibrium equations in constitutive stress-strain and

geometric compatibility were essentially followed in mechanical analysis. The change in temperature distribution influences the material characteristics and contributes to body deformation through thermal strains. Fluid flow modelling was not included since the effect of fluid flow on the deformation and stress field can be regarded minimal [33].

Thermo-physical material properties are imported into numerical simulation. The temperature-dependent properties for S235 as substrate material allocated in the FE model are shown in Fig. 7.

To achieve good result of coupled thermo-mechanical simulation, temperature-dependent properties of the filler material were required. Advanced material software JMAT-PRO was implemented to generate the thermo-mechanical and thermo-physical properties of stainless steel SS316L. As shown in Fig. 8, other principal temperature-dependent parameters such as heat conductivity coefficient, thermal expansion coefficient, specific heat capacity and modulus of elasticity are computed based on the chemical composition analysis from Table 2. These data were then entered into FEM software MSC Marc/Mentat for calculation.

The flow curve was described using plasticity model based on the isotropic hardening rule with von Mises yield criteria. The relationship between flow stress and true plastic strain in S235 and SS316L at strain rates of 0.01 s^{-1} and 0.001 s^{-1} is shown in Fig. 9.

3.2 Thermo-mechanical method for WAAM process: parameters, heat source and plasticity model

During WAAM process, the thermo-mechanical behaviours are complex since the simulation involves computing the deformations and stresses in the assigned material once thermal load is applied into the workpiece. Since welding processes can be seen as weakly coupled issues, TMM performance is usually solved in two steps [34]. At the initial stage, transient thermal analysis is carried out, and the nodal temperature histories from this analysis are then fed into the mechanical analysis.



Fig. 3. Investigation of substrate deformation using CMM Mitutoyo Beyond 707

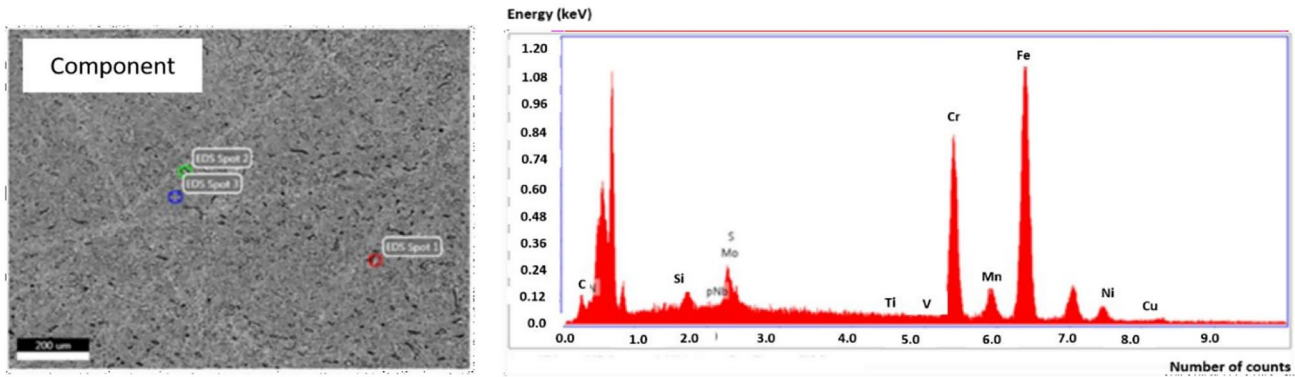


Fig. 4 SEM/EDX results of chemical composition on evolved SS316L component

Hence, it is possible to model transient distortions and residual stresses.

To model the moving welding heat source in this case, a time increment technique is employed to provide predictions that are similar to the real welding process. TMM assumes that thermal behaviour influences mechanical behaviour, while the mechanical response has no effect on the thermal history. Figure 10 describes a flow diagram of thermo-mechanical simulation of welding process. At time t_i , the thermal problem is solved first, followed by the application of thermal loading to the mechanical problem. The deposit geometry is modified by adding material properties at time t_{i+1} . The material properties are updated after each stable thermal iteration scheme. The prior computed data at t_i is used to initiate the thermal and mechanical problems. This updated material is used as input to the mechanical iteration scheme, where among others the stresses, strains and deformations are calculated. These two calculations are restarted over time t_{i+1} . The thermal issue is solved using an enthalpy formulation to allow numerical convergence due to the generated high temperature gradient with consideration of latent heat of fusion.

The thermal analysis is carried out utilizing a moving heat source and a heat conduction formulation with temperature-dependent thermal properties. The following is the governing equation for thermal analysis heat transfer during the WAAM process:

$$\rho c \frac{\partial T}{\partial t}(x, y, z, t) = -\nabla \cdot q(x, y, z, t) + Q(x, y, z, t) \quad (1)$$

where x, y and z are the coordinates in the reference system (mm), ρ is the density of the materials (g/mm^3), c is the

specific heat capacity ($\text{J g}^{-1} \text{ }^\circ\text{C}^{-1}$), T is the current temperature ($^\circ\text{C}$), ∇ is the spatial gradient operator, q is the heat flux (W/mm^2), Q is the heat input per unit volume (W/mm^3) and t is the time (s). The heat distribution through the body part using the temperature gradients is defined by Fourier’s equation of heat flux conduction:

$$q_{cond} = -k\nabla T \quad (2)$$

where k is the isotropic temperature-dependent thermal conductivity [$\text{J}/(\text{mms } ^\circ\text{C})$]. During the welding process, total heat losses owing to convection, thermal radiation or conduction through fixturing body sections may occur. Newton’s law of cooling defines heat loss due to convection (q_{conv}) as follows:

$$q_{conv} = h_{conv}(T_s - T_0) \quad (3)$$

where h_{conv} , T_s and T_0 are coefficient of heat transfer, surface temperature of the weldment and ambient temperature, respectively. The heat loss due to radiation is described by the Stefan-Boltzmann law as follows:

$$q_{rad} = \epsilon\sigma(T_s^4 - T_0^4) \quad (4)$$

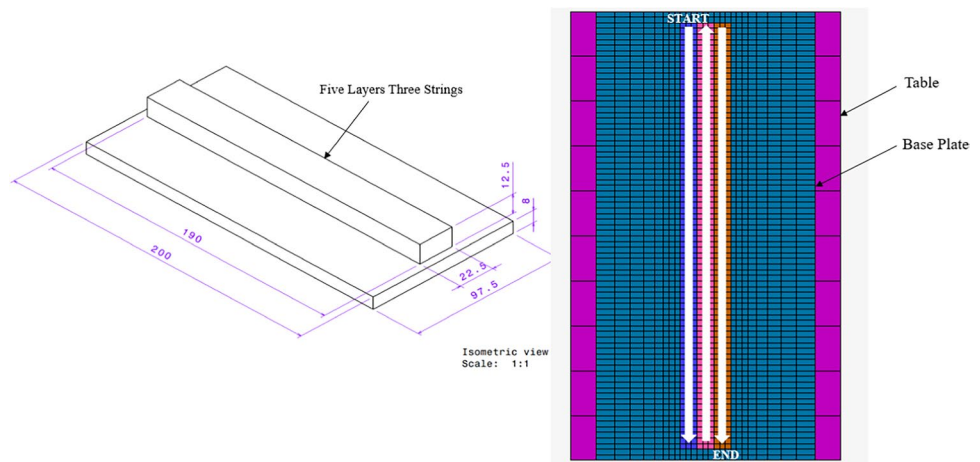
where ϵ and σ are surface emissivity and the Stefan-Boltzmann constant ($5.67 \times 10^{-8} \text{ W/m}^2\text{K}^4$), respectively. The ambient temperature in this study is set at $30 \text{ }^\circ\text{C}$. Table 3 summarizes all process parameters implemented in the numerical computation of WAAM model.

In WAAM, the heat source model is regarded as a critical parameter for thermal analysis. Hence, a suitable heat source model must be selected for any welding procedure. For GMAW process, the volumetric heat flux distributions (Q) as heat input around the welding pool are calculated

Table 2 Chemical composition of evolved component

Material	C	Cu	Cr	Mn	Mo	N	Ni	S	Si	Ti	V	P
Evolved component SS316L	0.03	0.76	17.83	2.43	1.63	-	10.57	-	0.63	0.267	0.3	-

Fig. 5 Geometrical model and welding direction of WAAM component



using Goldak’s double ellipsoid model. This model has been shown to accurately depict the heat power density from an electric arc traversing across the surface of a flat plate using GMAW process [35–37]. The geometrical features (a, b and c) on Goldak’s double ellipsoid heat source model as exhibited in Fig. 11 can be changed for the front or rear quadrants.

The subsequent equations were used to characterize the power density distribution inside the front and rear quadrants of the heat source along the welding path (z-axis). The power density of the heat flux in front and rear section ($Q_{f/r}$) of heat source can be modelled with Eq. (5).

The power density distribution inside the front and rear quadrants of the heat source (Q (f/r)) along the welding path was simulated using the Eq. (5).

$$Q_{f/r}(x, y, z) = \frac{6\sqrt{3}f_{f/r}Q}{abc_{f/r}\pi\sqrt{\pi}} e^{-3\frac{x^2}{a^2}} \cdot e^{-3\frac{y^2}{b^2}} \cdot e^{-3\frac{z^2}{c_{f/r}^2}} \quad (5)$$

Principally, the of heat flux distributions in this model is determined by four directions which width (a), depth

(b), rear length (c_r) and front length (c_f) [38]. The fractions of the deposition heads f_f and f_r denote the heat distribution of the heat flux in the front and rear quadrants by taking assumption that the condition $f_f + f_r = 2$ is fulfilled. These fractions can be assumed to be $f_f = \frac{2c_f}{c_f+c_r}$ and $f_r = \frac{2c_r}{c_f+c_r}$ if the volumetric heat source is treated as the equation of power density for the moving heat source. The numerical computation approach was based on the authors' earlier research with further improvement to achieve a better outcome [28], and the value of each direction is implemented in the simulation of GMAW. Table 4 shows the dimension and value for each direction.

The mechanical analysis is carried out using the thermal analysis or temperature field as an input. The non-linear stress-strain curve is modelled using the isotropic strain hardening rule with the von Mises yield criterion to calculate the stress and deformation [40]. Equation (6) represents mathematical expression of the total strain increment $\Delta\epsilon$ for mechanical analysis.

Fig. 6 The boundary conditions with industrial clamping locations

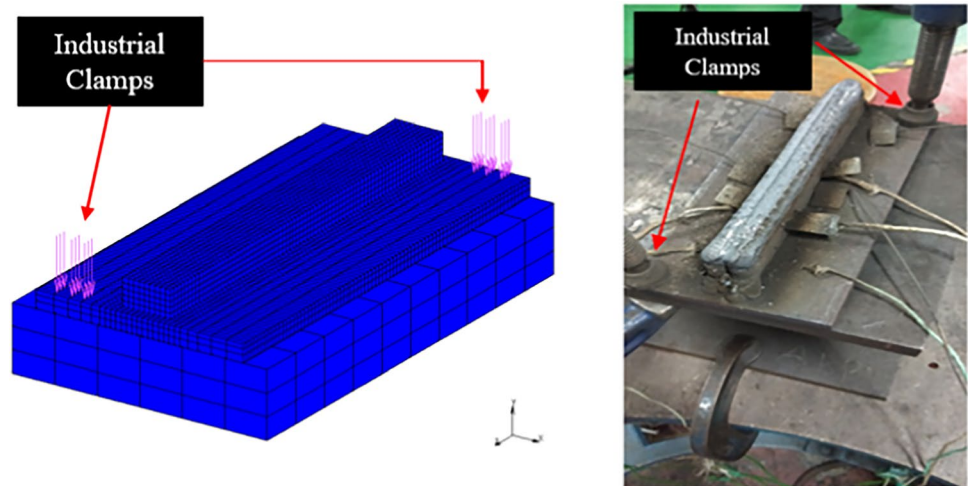
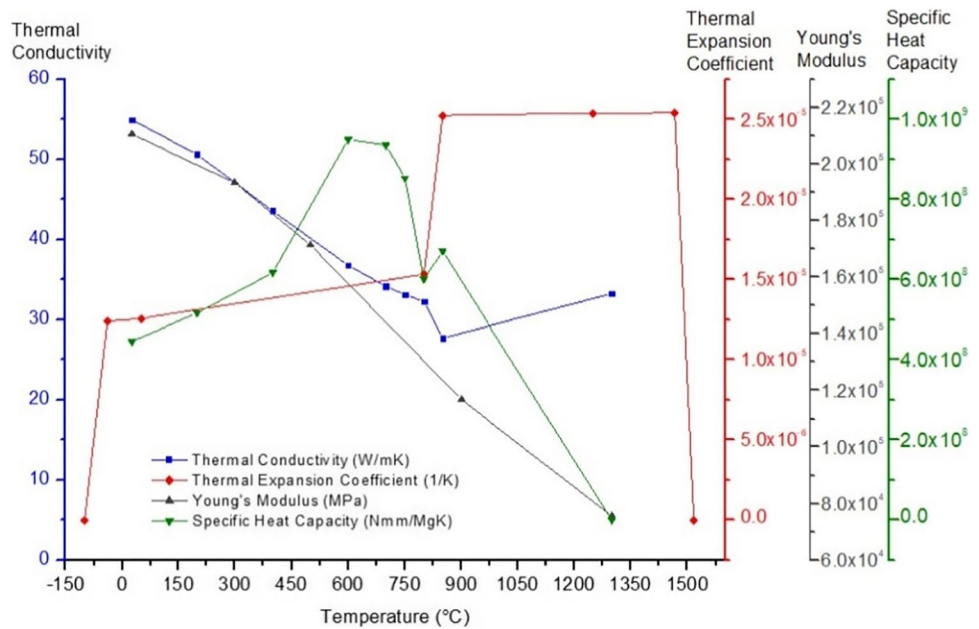


Fig. 7 Thermo-mechanical properties of S235



$$\Delta\epsilon = \Delta\epsilon^{elastic} + \Delta\epsilon^{plastic} + \Delta\epsilon^{thermal} + \Delta\epsilon^{creep} + \Delta\epsilon^{phase} \quad (6)$$

where $\Delta\epsilon^{elastic}$, $\Delta\epsilon^{plastic}$, $\Delta\epsilon^{thermal}$, $\Delta\epsilon^{creep}$ and $\Delta\epsilon^{phase}$ are increments for elastic, plastic, thermal, creep and phase transformation strain, respectively. In this study, the phase transformation-related and creep strain were ignored since it makes a minor contribution to total strain in austenitic stainless steel SS316L and the heating time in WAAM is considerably short.

The model of plasticity is defied by three parameters which are yield criterion, flow rule and hardening law [41,

42]. The von Mises yield criterion, provided by Eq. (7), is the most extensively used plasticity model by many researchers where σ_1, σ_2 and σ_3 are the principal stresses [43–47]. According to the flow rule, the plastic flow and the yield surface are orthogonal to each other.

$$\sigma_y = \sqrt{\frac{(\sigma_1 - \sigma_2)^2 + (\sigma_2 - \sigma_3)^2 + (\sigma_3 - \sigma_1)^2}{2}} \quad (7)$$

To calculate the amount of plastic flow and the evolution of the material’s yield strength, a hardening law is necessary.

Fig. 8 Thermo-mechanical properties of components of SS316L

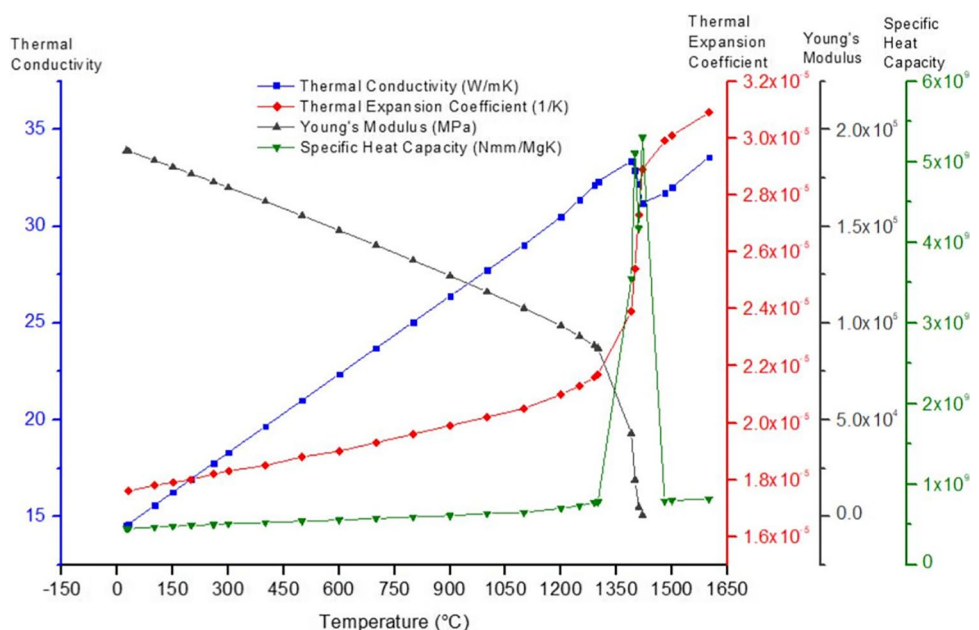
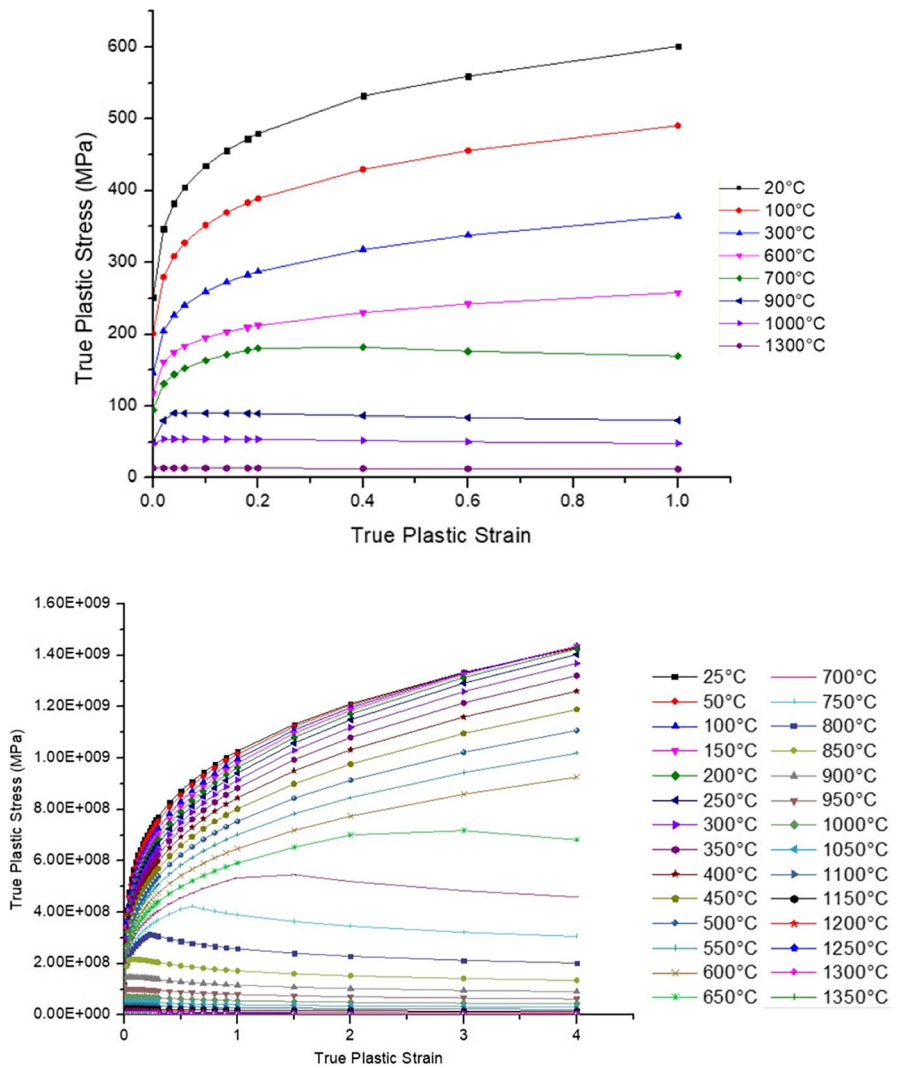


Fig. 9 The flow curves of material S235 (top) and SS316L (bottom)



A hardening law is required to determine the amount of plastic flow and the evolution of the yield strength of the material [21]. In this study, the isotropic hardening law is implemented to simulate a WAAM model without taking

phase transformation into account. Equation (8) depicts the relationship between the assigned material’s stress and strain.

$$\sigma = \sigma_y + H(\epsilon^P)^N \tag{8}$$

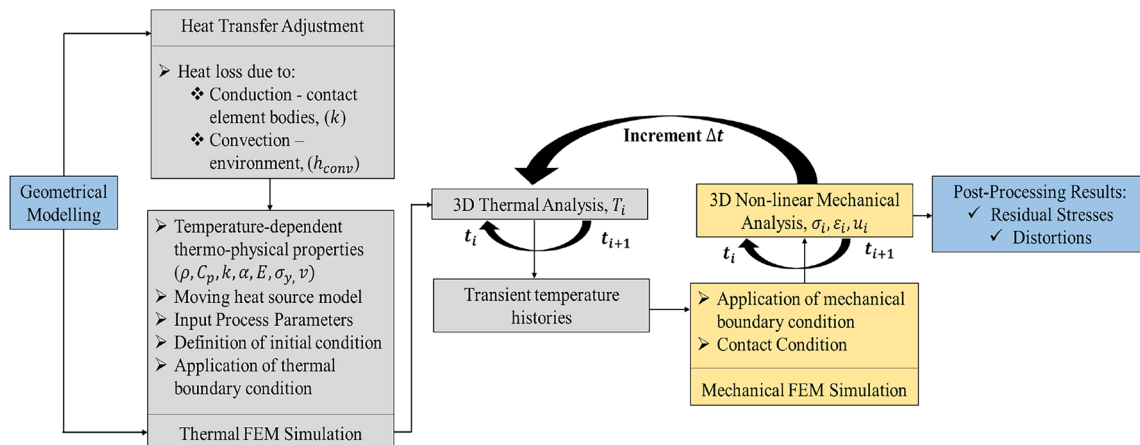


Fig. 10 Flow diagram of coupled thermo-mechanical analysis

Table 3 Process parameters implemented in TMM-based simulation on WAAM

Process parameters and physical properties	Value
Current (I)	172 A
Voltage (V)	19.8 V
Efficiency (η)	0.8
Travel speed (v)	5 mm/s
Latent heat	256400 J/kg
Solidus temperature	1279 °C
Liquidus temperature	1450 °C

where σ , σ_y , H , ϵ^p and N are total stress, initial yield stress, hardening law coefficient, plastic strain and hardening law exponent, respectively.

3.3 Thick-walled WAAM simulation with thermal calibration

The applied welding strategy has primary influence on the temperature distribution in the weld layers as well as in the substrate. The usage of thermocouples in the real experiment was aimed to calibrate the numerical computational analysis, especially for the heat transfer coefficients to the environment and to the other components.

The measured and simulated temperature for thick-walled WAAM of stainless steel SS316L is shown in Fig. 12. The temperature history was taken by the thermocouple at base plate and the second layer of weld bead on approximately 85 mm before the end of the weld bead. During the measurement in the filler material, the comparison between simulation and actual experiment revealed that the maximum temperature cannot be determined. This is due to the fact that the thermocouples were not intended for the steel’s melting point and the measuring sensors’ inertia was not designed to capture the short-term maximum temperature. Temperature measurement with thermocouples, on the other hand, was critical for describing

Table 4 Heat source dimension of Goldak’s double ellipsoid applied in FEM

Dimension of heat source	Value
Width (a)	7.5 mm
Depth (b)	5 mm
Front length (c_f)	4 mm
Rear length (c_r)	10 mm

the cooling and reheating behaviour of layers. Therefore, attempts to analyse the thermal behaviour shall be carried out accordingly and compared with the simulated results.

3.4 Mesh sensitivity analysis

The quantity and size of FEM meshes have a significant impact on the model’s accuracy and computational time. In the similar condition, smaller meshes in the model are expected to produce more accurate results. However, performing the operation will necessitate a longer computational time and a large amount of data storage space. As a result, a balanced meshing strategy should be employed to achieve appropriate accuracy in the temperature and stress fields while using the optimized number of elements in the model.

A mesh sensitivity was analysed to determine the proper meshing for the model. The investigation was carried out on eight different constructed models with varying meshing density. The length, width and thickness of the base plate designed in this study were similar to those used in the experiment, which were 200 mm, 97.5 mm and 8 mm, respectively. Because the weld metal and the heat-affected zone suffer substantial temperature gradients, finer meshes were used in this area. In the x-direction, the weld bead and heat-affected zone element models were subdivided with widths of 7.5 mm, 3.75 mm, 2.5 mm and 1.25 mm. A simplified WAAM component was additively modelled with only two layers and three strings to save computational time for the mesh sensitivity study. After the last deposition, the final load case was configured with holding time of 240 s to compute the cooling process of WAAM components. Model 1 and model 2 are the coarser and finer element mesh models, respectively, as shown in Fig. 13. All of material properties, heat source model and thermal boundary conditions were set up in the similar way as described in the previous section.

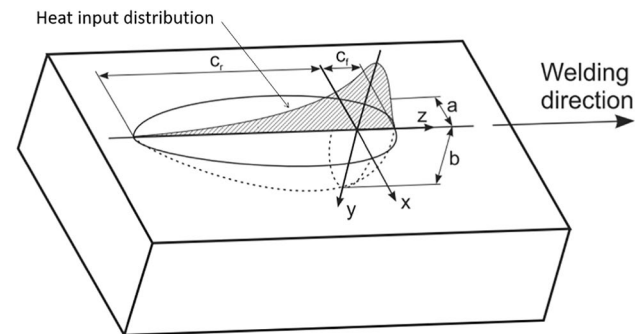
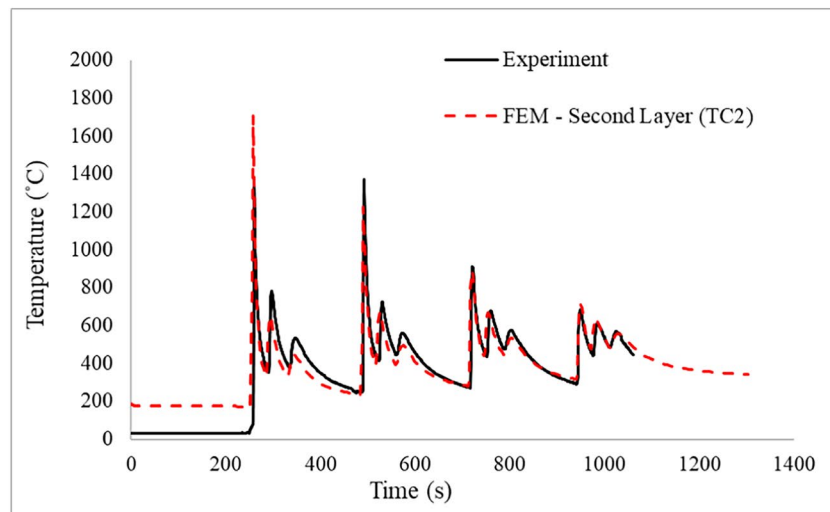
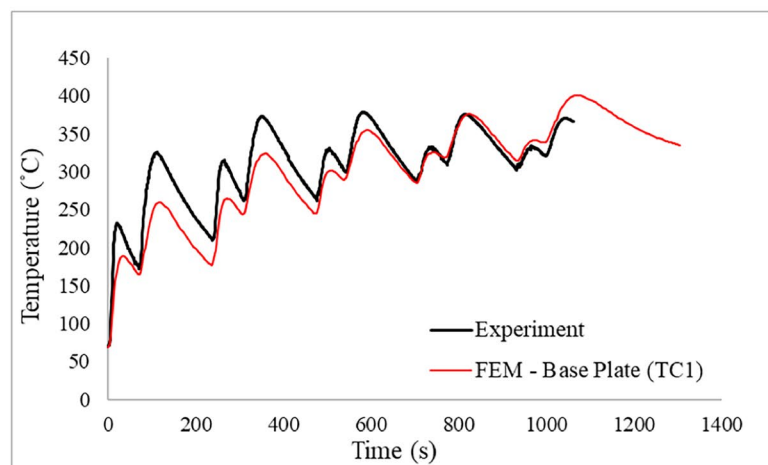
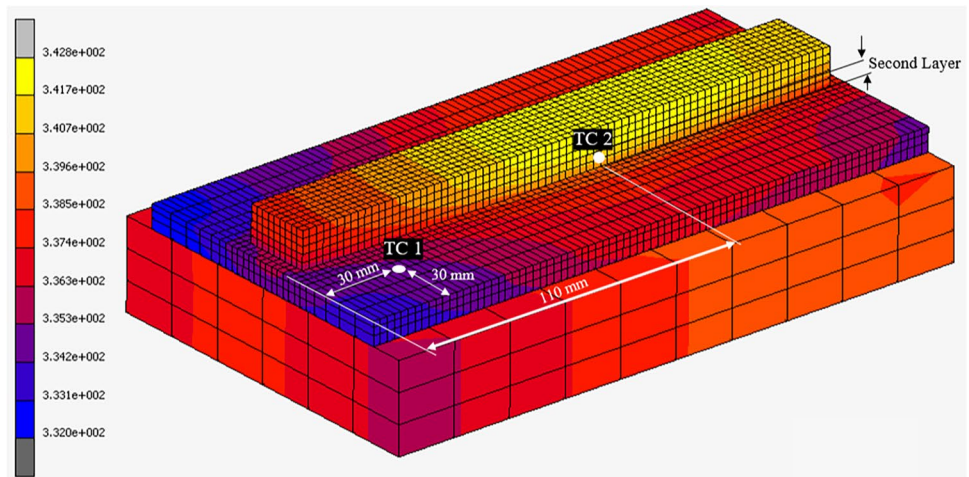


Fig. 11 Illustration of Goldak’s double ellipsoid heat source model

4 Result and discussions

While the inconsistent time steps of the recording device triggered a small discrepancy between the experimental and numerical results for thermal calibration, the boundary conditions and time increments in FEM were known as idealized and constant. The heat transfer coefficients for

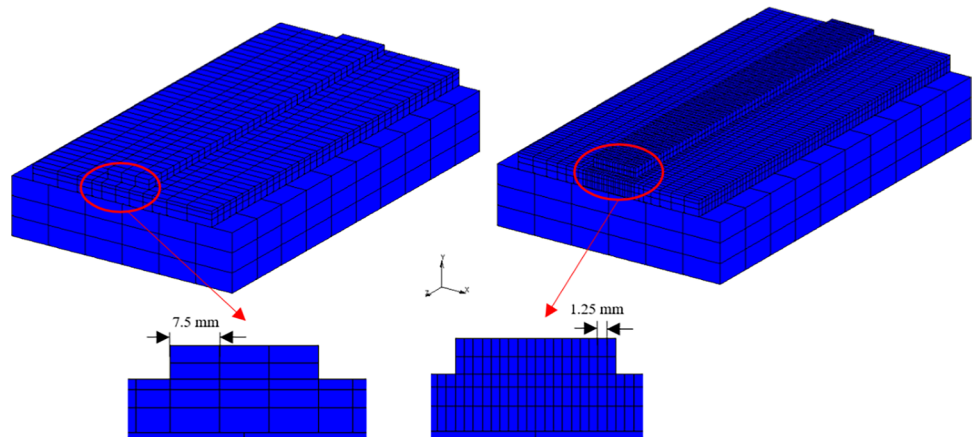
Fig. 12 Thermal calibration of WAAM components: Thermocouple location (top), temperature distribution (TC1) on base plate (middle) and TC2 at second layer (bottom)



metal-to-metal and metal-to-environment were adjusted to examine the temperature distribution. The adjusted thermal boundary conditions, which were implemented in the

numerical calculation, are summarized in Table 5. The modified values differ from those frequently taken from software database.

Fig. 13 Coarse model 1 with 1728 elements (left) and finer model 2 with 11556 elements (right)



The result of sensitivity analysis shows that if the number of elements reaches over 5000, the maximum temperature continuous almost constantly equal at ca. 1350 °C. Opposite to that, the maximum temperature obtained for models with fewer elements exhibits approximately 10–15% error compared to experimental study. For this, the element size of 2.5 mm was selected to model the nearby and weld bead area in simulating the full WAAM component of five layers and three strings. Figure 14 illustrates the maximum temperature for different numbers of element.

In order to verify the results between experiment and simulation, a comparative study was conducted. Figure 15 exhibits a contour band model displaying the substrate displacement result of FEM simulation in y-direction. In order to predict a significant substrate deformation of numerical simulation, a special load case was assigned at the very end of the FEM step procedure for removing the exerted clamps and worktable. This was accomplished to simulate actual WAAM conditions as closely as possible. Based on the result, the substrate deformation increases once the clamping loads have been removed. For analysing the mechanical results, the predicted angular substrate deformation along the edge on eleven different points was measured by using CMM Mitutoyo Beyond 707.

Figure 16 exhibits the comparative results between experiment and simulation with the percentage error. It can be seen that both experimental and simulated data have fairly similar profile in displacements. This finding can be explained that using material modelling based on the actual evolved welded component permits a high degree

correlation between the simulated and measured deformation pattern.

The highest distortions occur at the unclamped area, and the discrepancy in distortion values appears to be in the range of 0.003 to 0.161 mm. This discrepancy in the correlation between the displacements of the FE models and the experimental results can be due to the fluctuating WAAM process parameters and complex non-linearity of thermo-mechanical material properties. Despite some deviations in weld deformation, the simulated data shows a good agreement with the experiment. It can be observed that the total substrate deformation results between thermo-mechanical FEM simulation of WAAM process and experimental study depict relative percentage errors up to 10.1% at each particular measurement points in average.

Based on the Fig. 16, it can also be seen than the maximum distortion is symmetrically at the edges without clamping. Although the distortion on the other side of the plate was not measured numerically, without any doubt the simulation result is acceptable since the numerical error is within the acceptable range as a result of several experimental attempts.

Table 5 Adjusted coefficient values for WAAM model with thick wall

Thermal boundary conditions	Value
Heat transfer coefficient (metal to metal)	2500 W/m ² /K
Heat transfer coefficient (metal to environment)	15 W/m ² /K

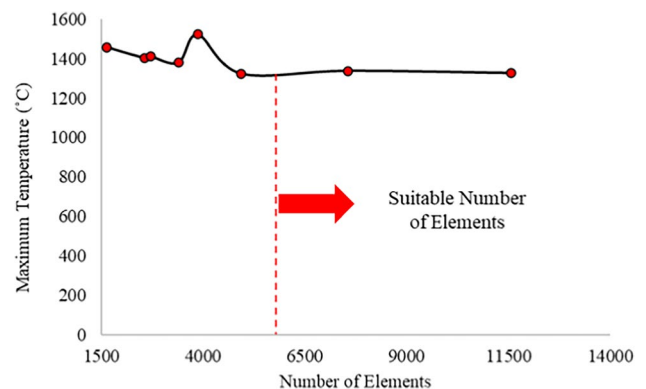


Fig. 14 Mesh sensitivity analysis of two layers three strings WAAM process

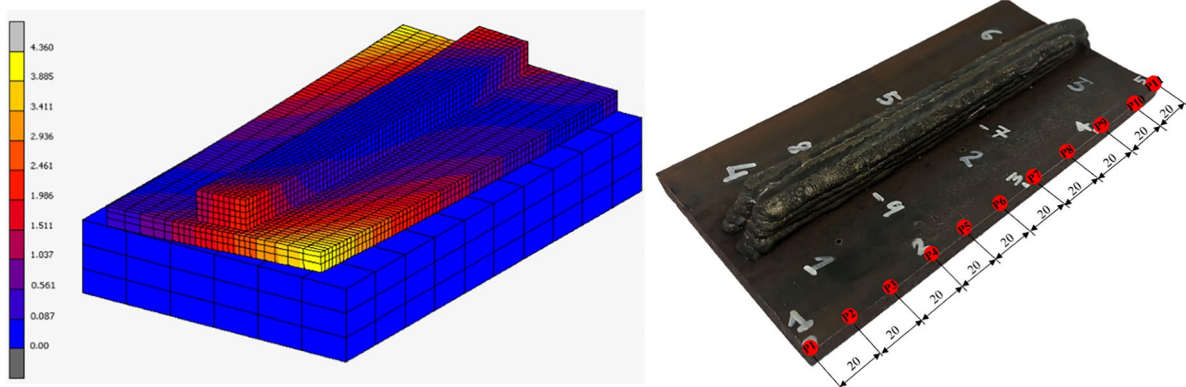
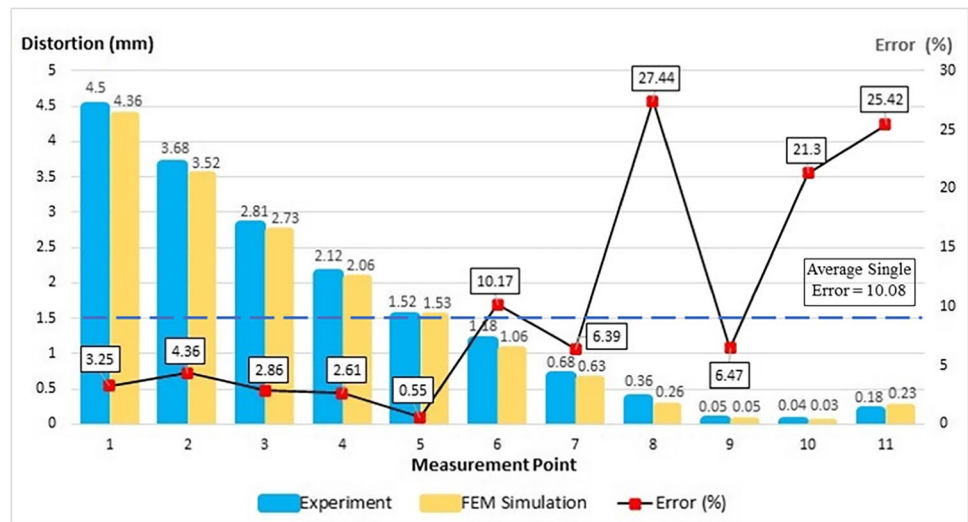


Fig. 15 Substrate deformation in y-direction of WAAM model (left) and location of measurement points on WAAM experiment (right)

Fig. 16 Comparison of substrate deformation of FEM simulation and experiment



5 Conclusion and further recommendation

This research was an advancement of previous works conducted by authors using simulation [28, 39] and experiment [48]. The primary objective of this research was to investigate the correlations between process parameters setting, materials modelling and clamping conditions on the thermo-mechanical behaviour of WAAM substrate of SS316L using numerical computation and experimental study. For realistic FEM simulation and better accuracy results, it is significant to determine first the temperature-dependent material properties of actual heated wire feedstock of SS316L that employed in the experiment. Hence, considering adjusted heat transfer coefficient applied in the numerical simulation plays important role to calibrate the thermal cycles of WAAM process of SS316L.

The numerical analysis for five layers and three strings of thick-walled WAAM component and the experimental

WAAM process using the structured approach were both completed successfully. The thermo-mechanical and thermo-physical properties were obtained experimentally and computed using material modelling software based on chemical composition analysis. In this FEM simulation, rectangular shape geometrical bead modelling was applied for WAAM model which can reduce the computational time caused by simpler meshing with determined elements number according to sensitivity analysis.

For the thermal calibration, thick-walled WAAM model by numerical simulation gives accurate forecast of the temperatures profile considering the thermal boundary conditions as the numerical parameters. By comparing the simulation and experiment of WAAM, the total substrate distortion results display error percentages up to 10.08% on specific points. The difference between the measured and computed temperature and substrate distortion results could be due to non-homogeneous material, non-linear geometry, pre-conditioning and parameter

changes during actual WAAM application. Actual bead irregularity can lead to distortion which is created by localized heating of the substrate causing local expansion and contractions during WAAM process. Residual stresses might build up due to repetitive different weld thermal cycle during heating and cooling stages of welding operations experienced by the substrate.

As further research, following recommendation can be proposed:

1. Implementation of more advanced measurement device for analysing elemental composition, for example, by using GD-OES (glow discharge optical emission spectroscopy).
2. Investigation on heat source model using a rectangular model could be taken into consideration within in FEM simulation so that an optimum result could be expected in term of deformations.
3. Observation using numerical computation and experiment of more complex component and substrate geometry.
4. Analyzation of other materials.

Acknowledgements The authors would like to express their gratitude to staff members of Smart Manufacturing Research Institute (SMRI) and Research Interest Group: Advanced Manufacturing Technology (RIG:AMT) at School of Mechanical Engineering, Universiti Teknologi MARA (UiTM) Shah Alam for encouraging this research. Some data and results were obtained partially from previous investigations conducted by the group members of Section “Engineering Materials – Grain Growth” led by Mr. Muhd Faiz bin Mat @ Muhammad who had presented in various conferences.

Funding This research is also financially supported by ASEA-UNET grant with the project number ASEA 2019/Montan/1, ERASMUS+ (Montan University in Leoben), Geran Penyelidikan Khas (GPK) with Project Code: 600-RMC/GPK 5/3 (123/2020), Geran Konsortium Kecemerlangan Penyelidikan (Large Volume Additive Manufacturing/LVAM) from Ministry of Higher Education (MOHE) in Malaysia and TechnoGerma Engineering & Consulting Sdn. Bhd.

Declarations

Ethics approval This article does not contain any studies with human participants or animals performed by any of the authors.

Consent to participate Not applicable.

Consent for publication Not applicable.

Conflict of interest The authors declare no competing interests.

References

1. Jiang J, Ma Y (2020) Path planning strategies to optimize accuracy, quality, build time and material use in additive manufacturing: a review. *Micromachines* 11(7):663. <https://doi.org/10.3390/MII1070633>
2. Jiang J, Newman ST, Zhong RY (2021) A review of multiple degrees of freedom for additive manufacturing machines. *Int J Comput Integr Manuf* 34(2):195–211. <https://doi.org/10.1080/0951192X.2020.1858510>
3. Frazier WE (2014) Metal additive manufacturing: a review. *J Mater Eng Perform* 23(6):1917–1928. <https://doi.org/10.1007/s11665-014-0958-z>
4. Derekar KS (2018) A review of wire arc additive manufacturing and advances in wire arc additive manufacturing of aluminium. *Mater Sci Technol (United Kingdom)* 34(8):895–916. <https://doi.org/10.1080/02670836.2018.1455012>
5. Ford S, Despeisse M (2016) Additive manufacturing and sustainability: an exploratory study of the advantages and challenges. *J Clean Prod* 137:1573–1587. <https://doi.org/10.1016/j.jclepro.2016.04.150>
6. Li R, Kim YS, Van Tho H, Yum YJ, Kim WJ, Yang SY (2019) Additive manufacturing (AM) of piercing punches by the PBF method of metal 3D printing using mold steel powder materials. *J Mech Sci Technol* 33(2):809–817. <https://doi.org/10.1007/s12206-019-0137-0>
7. Ogino Y, Asai S, Hirata Y (2018) Numerical simulation of WAAM process by a GMAW weld pool model. *Weld World* 62:393–401. <https://doi.org/10.1007/s40194-018-0556-z>
8. Williams SW, Martina F, Addison AC, Ding J, Pardal G, Colegrove P (2016) Wire + Arc additive manufacturing. *Mater Sci Technol (United Kingdom)* 32(7):641–647. <https://doi.org/10.1179/1743284715Y.0000000073>
9. Liberini M, Astarita A, Campatelli G, Scippa A, Montevecchi F, Venturini G, Squillace A (2017) Selection of optimal process parameters for wire arc additive manufacturing. *Procedia CIRP* 62:470–474. <https://doi.org/10.1016/j.procir.2016.06.124>
10. Rodrigues TA, Duarte V, Miranda RM, Santos TG, Oliveira JP (2019) Current status and perspectives on wire and arc additive manufacturing (WAAM). *Materials* 12(7):1121. <https://doi.org/10.3390/ma1207112>
11. Ding D, Pan Z, Cuiuri D, Li H (2015a) Wire-feed additive manufacturing of metal components: technologies, developments and future interests. *Int J Adv Manuf Technol* 81(1-4):465–481. <https://doi.org/10.1007/s00170-015-7077-3>
12. Ding D, Pan Z, Cuiuri D, Li H (2015b) A practical path planning methodology for wire and arc additive manufacturing of thin-walled structures. *Robot Comput Integr Manuf* 34:8–19. <https://doi.org/10.1016/j.rcim.2015.01.003>
13. Bonifaz EA, Palomeque JS (2020) A mechanical model in wire + Arc additive manufacturing process. *Prog Addit Manuf* 5(2):63–169. <https://doi.org/10.1007/s40964-020-00112-y>
14. Hu Z, Qin X, Li Y, Yuan J, Wu Q (2020) Multi-bead overlapping model with varying cross-section profile for robotic GMAW-based additive manufacturing. *J Intell Manuf* 31:1133–1147. <https://doi.org/10.1007/s10845-019-01501-z>
15. Fude W, Stewart W, Matthew R (2011) Morphology investigation on direct current pulsed gas tungsten arc welded additive layer manufactured Ti6Al4V alloy. *Int J Adv Manuf Technol* 57(5–8):597–603. <https://doi.org/10.1007/s00170-011-3299-1>
16. Brandl E, Baufeld B, Leyens C, Gault R (2010) Additive manufactured Ti-6Al-4V using welding wire: comparison of laser and arc beam deposition and evaluation with respect to aerospace material specifications. *Phys Procedia* 5:595–606. <https://doi.org/10.1016/j.phpro.2010.08.087>
17. Wang C, Kim JW (2018) Numerical analysis of distortions by using an incorporated model for welding-heating-cutting processes of a welded lifting lug. *J Mech Sci Technol* 32(12):5855–5862. <https://doi.org/10.1007/s12206-018-1134-4>
18. Chua BL, Lee HJ, Ahn DG, Kim JG (2018) Influence of process parameters on temperature and residual stress distributions

- of the deposited part by a Ti-6Al-4V wire feeding type direct energy deposition process. *J Mech Sci Technol* 32(11):5363–5372. <https://doi.org/10.1007/s12206-018-1035-6>
19. Xiong J, Li R, Lei Y, Chen H (2018) Heat propagation of circular thin-walled parts fabricated in additive manufacturing using gas metal arc welding. *J Mater Process Technol* 251:12–19. <https://doi.org/10.1016/j.jmatprotec.2017.08.007>
 20. Awiszus B, Mayr P, Graf M, Hälsig A, Höfer K (2018) Thermo-mechanical modelling of wire-arc additive manufacturing (WAAM) of semi-finished products. *Metals* 8(12):1009. <https://doi.org/10.3390/met8121009>
 21. Ding J, Colegrove P, Mehnen J, Williams S, Wang F, Almeida PS (2014) A computationally efficient finite element model of wire and arc additive manufacturing. *Int J Adv Manuf Technol* 70:227–236. <https://doi.org/10.1007/s00170-013-5261-x>
 22. Islam M, Buijk A, Rais-Rohani M, Motoyama K (2014) Simulation-based numerical optimization of arc welding process for reduced distortion in welded structures. *Finite Elem Anal Des* 84:54–64. <https://doi.org/10.1016/j.finel.2014.02.003>
 23. Ríos S, Colegrove PA, Martina F, Williams SW (2018) Analytical process model for wire + arc additive manufacturing. *Addit Manuf* 21:651–657. <https://doi.org/10.1016/j.addma.2018.04.003>
 24. Graf M, Pradjadhiana KP, Hälsig A, Manurung YHP, Awiszus B (2018) Numerical simulation of metallic wire arc additive manufacturing (WAAM). *AIP Conference Proceedings* 1960(1). <https://doi.org/10.1063/1.5035002>
 25. Jia J, Zhao Y, Dong M, Wu A, Li Q (2020) Numerical simulation on residual stress and deformation for WAAM parts of aluminum alloy based on temperature function method. *China Weld* 29(2):1–8. <https://doi.org/10.12073/j.cw.20191101002>
 26. Montevecchi F, Venturini G, Scippa A, Campatelli G (2016) Finite element modelling of wire-arc-additive-manufacturing process. *Procedia CIRP* 55:109–114. <https://doi.org/10.1016/j.procir.2016.08.024>
 27. Depradeux L, Jullien JF (2004) 2D and 3D numerical simulations of TIG welding of a 316L steel sheet. *Rev Eur Des Elem* 13(3–4):269–288. <https://doi.org/10.3166/reef.13.269-288>
 28. Ahmad SN, Manurung YHP, Mat MF, Leitner M (2021) Investigation of material property model on substrate deformation induced by thick-walled WAAM process using numerical computation. *Lect Notes Mech Eng* 46:747–761. <https://doi.org/10.1007/978-981-15-9505-9>
 29. Israr R, Buhl J, Elze L, Bambach M (2018) Simulation of different path for WAAM with Lagrangian finite element methods. *15.LS-DYna Forum* 2018, Bamberg
 30. Wang C, Kim YR, Kim JW (2014) Comparison of FE models to predict the welding distortion in T-joint gas metal arc welding process. *Int J Precis Eng Manuf* 15(8):1631–1637. <https://doi.org/10.1007/s12541-014-0513-8>
 31. Montevecchi F, Venturini G, Grossi N, Scippa A, Campatelli G (2017) Finite element mesh coarsening for effective distortion prediction in wire arc additive manufacturing. *Addit Manuf* 18:145–155. <https://doi.org/10.1016/j.addma.2017.10.010>
 32. Velaga SK, Ravisankar A (2017) Finite element based parametric study on the characterization of weld process moving heat source parameters in austenitic stainless steel. *Int J Press Vessel Pip* 157:63–73. <https://doi.org/10.1016/j.ijpvp.2017.09.001>
 33. Goldak JA, Akhlaghi M (2005) *Computational welding mechanics*. Springer International Publishing, US. <https://doi.org/10.1007/b101137>
 34. Ding J (2012) *Thermo-mechanical analysis of wire and arc additive manufacturing Process School*, Cranfield University
 35. Darmadi DB, Tieu AK, Norrish J (2012) A validated thermal model of bead-on-plate welding. *Heat Mass Transf* 48(7):1219–1230. <https://doi.org/10.1007/s00231-012-0970-5>
 36. Kollár D, Kövesdi B, Vigh LG, Horváth S (2019) Weld process model for simulating metal active gas welding. *Int J Adv Manuf Technol* 102(5–8):2063–2083. <https://doi.org/10.1007/s00170-019-03302-3>
 37. Reda R, Magdy M, Rady M (2020) Ti-6Al-4V TIG weld analysis using FEM simulation and experimental characterization. *Iran J Sci Technol Trans Mech Eng* 44(3):765–782. <https://doi.org/10.1007/s40997-019-00287-y>
 38. Goldak J, Chakravarti A, Bibby M (1984) A new finite element model for welding heat sources. *Metall Trans B* 15(2):299–305. <https://doi.org/10.1007/BF02667333>
 39. Ahmad SN (2020) FEM simulation procedure for distortion and residual stress analysis of wire arc additive manufacturing. *IOP Conf Ser Mater Sci Eng* 834(1). <https://doi.org/10.1088/1757-899X/834/1/012083>
 40. Zain-ul-abdein M, Nélias D, Jullien JF, Deloison D (2010) Experimental investigation and finite element simulation of laser beam welding induced residual stresses and distortions in thin sheets of AA 6056-T4. *Mater Sci Eng A* 527(12):3025–3039. <https://doi.org/10.1016/j.msea.2010.01.054>
 41. Lindgren LE (2001) Finite element modeling and simulation of welding part 2: Improved material modeling. *J Therm Stress* 24(3):195–231. <https://doi.org/10.1080/014957301300006380>
 42. Theofilos-Ioannis M (2012) Elastoplastic constitutive models in finite element analysis. National Technical University Athens
 43. Malik AM, Qureshi EM, Dar NU, Khan I (2008) Analysis of circumferentially arc welded thin-walled cylinders to investigate the residual stress fields. *Thin-Walled Struct* 46(12):1391–1401. <https://doi.org/10.1016/j.tws.2008.03.011>
 44. Asserin O, Loredo A, Petelet M, Iooss B (2011) Global sensitivity analysis in welding simulations - what are the material data you really need. *Finite Elem Anal Des* 47(9):1004–1016. <https://doi.org/10.1016/j.finel.2011.03.016>
 45. Qureshi EM, Malik AM, Dar NU (2009) Residual stress fields due to varying tack welds orientation in circumferentially welded thin-walled cylinders. *Adv Mech Eng* 2009(10):1–9. <https://doi.org/10.1155/2009/351369>
 46. Pasternak H, Launert B, Krausche T (2015) Welding of girders with thick plates - fabrication, measurement and simulation. *J Constr Steel Res* 115:407–416. <https://doi.org/10.1016/j.jcsr.2015.08.037>
 47. Wang Q, Liu XS, Wang P, Xiong X, Fang HY (2017) Numerical simulation of residual stress in 10Ni5CrMoV steel weldments. *J Mater Process Technol* 240:77–86. <https://doi.org/10.1016/j.jmatprotec.2016.09.011>
 48. Mat MF, Manurung YHP, Muhammad N, Ahmad SN, Leitner M (2021) Grain growth prediction of SS316l stainless steel of bead-on-plate using numerical computation. *Lect Notes Mech Eng* 46:1–11. <https://doi.org/10.1007/978-981-15-9505-9>

Publisher's Note Springer Nature remains neutral with regard to jurisdictional claims in published maps and institutional affiliations.